CITATION

Klymak, J.M., S. Legg, M.H. Alford, M. Buijsman, R. Pinkel, and J.D. Nash. 2012. The direct breaking of internal waves at steep topography. *Oceanography* 25(2):150–159, http://dx.doi.org/10.5670/oceanog.2012.50.
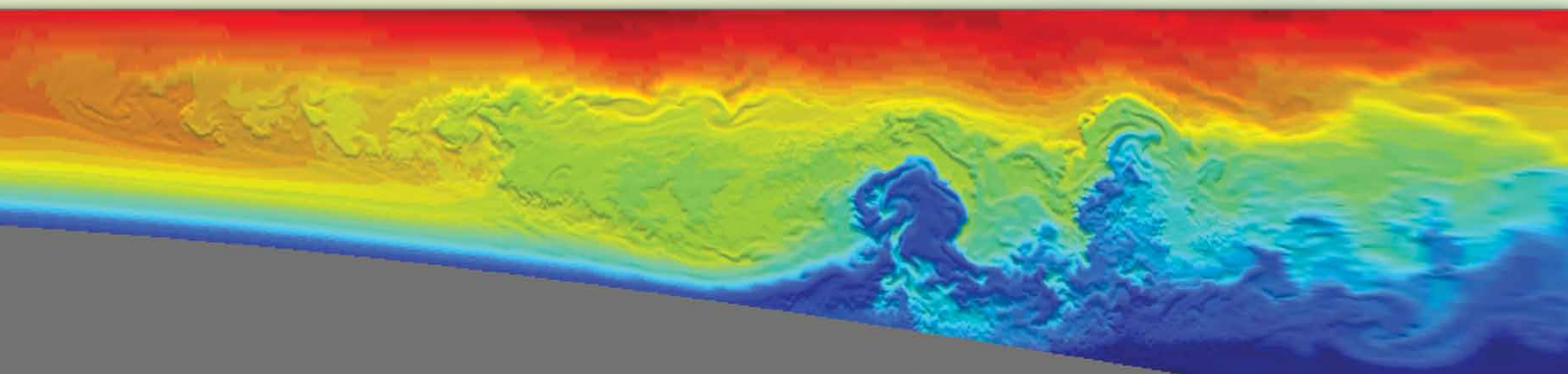
DOI

http://dx.doi.org/10.5670/oceanog.2012.50

The Direct Breaking of Internal Waves at Steep Topography

BY JODY M. KLYMAK, SONYA LEGG, MATTHEW H. ALFORD,

MAARTEN BUIJSMAN, ROBERT PINKEL, AND JONATHAN D. NASH

ABSTRACT. Internal waves are often observed to break close to the seafloor topography that generates them, or from which they scatter. This breaking is often spectacular, with turbulent structures observed hundreds of meters above the seafloor, and driving turbulence dissipations and mixing up to 10,000 times open-ocean levels. This article provides an overview of efforts to observe and understand this turbulence, and to parameterize it near steep "supercritical" topography (i.e., topography that is steeper than internal wave energy characteristics). Using numerical models, we demonstrate that arrested lee waves are an important turbulence-producing phenomenon. Analogous to hydraulic jumps in water flowing over an obstacle in a stream, these waves are formed and then break during each tidal cycle. Similar lee waves are also observed in the atmosphere and in shallow fjords, but in those cases, their wavelengths are of similar scale to the topography, whereas in the ocean, they are small compared to the water depth and obstacle size. The simulations indicate that these nonlinear lee waves propagate against the generating flow (usually the tide) and are arrested because they have the same phase speed as the oncoming flow. This characteristic allows estimation of their size a priori and, using a linear model of internal tide generation, computation of how much energy they trap and turn into turbulence. This approach yields an accurate parameterization of mixing in numerical models, and these models are being used to guide a new generation of observations.

INTRODUCTION

Internal waves transmit energy to the ocean's interior. In order to affect the mean flow and the mixing of nutrients in the ocean, these waves must, by some mechanism, break and become turbulent. The resulting mixing creates lateral density gradients that drive ocean currents, both local and on the scale of the global thermohaline circulation. It has been estimated that the deep ocean requires 2 TW of energy to maintain the observed overturning circulation, and that this energy can be supplied approximately equally by internal waves forced by wind and by tides (Munk and Wunsch, 1998). Tracking the energy pathways of internal waves generated by winds is difficult because they are

spatially variable and sporadic (D'Asaro, 1995; Alford, 2003), but recent progress has been made on understanding the energy balance of tides.

Though simpler than wind-driven waves, the energy balance of internal tides is still quite complex (Figure 1). Internal tides are generated when the surface tide pushes density-stratified water over topography, creating internal pressure gradients that drive the waves. In the bounded ocean, the waves propagate away from the topography in vertical "modes." The lowest internal wave mode has the longest vertical wavelength that can fit between the surface and the seafloor, and is analogous to the resonant note in a pipe organ or guitar string. In an internal wave, this means that the lowest mode has the strongest velocities at the surface and seafloor and null velocity in the middle of the water column, and it propagates with a horizontal phase speed that is faster than higher modes. Higher modes have more zero crossings and travel at slower speeds. This response can be seen in the top panel of Figure 1, early in a numerical tidal simulation, where the low modes have traveled almost 500 km from the ridge at x = 0, but the more complicated "high-mode" structure is just starting to form near the ridge. The high modes may break into turbulence locally where they are generated (Figure 1, lower panel), at remote topography (Nash et al., 2004), or by wave-wave interactions in the interior (Henyey et al., 1986; St. Laurent et al., 2002; Polzin, 2009; MacKinnon and Winters, 2005). Low modes can reflect, interfere with one another, and scatter into higher modes, though which

processes dominate at any given location is not understood.

Steepness of the topography is an important factor in the study of topographic interactions with internal waves (Garrett and Kunze, 2007). As can be seen emanating from the topography in Figure 1, internal waves organize along "beams" of energy, which propagate at characteristic angles that depend on the frequency of the waves and the density stratification. If the topography is gentler than these characteristic slopes, it is said to be "subcritical;" if steeper, it is said to be "supercritical." Of course, real topography has regions of both, but the extremes are useful because mathematical predictions of internal tide generation can be formulated for either assumption (for subcritical topography, see Bell, 1975, and Balmforth et al., 2002; for supercritical topography, see Llewellyn Smith and Young, 2003, and St. Laurent et al., 2003).

At regions of subcritical topography, such as the Brazil Basin, internal tide

generation is relatively linear. Nonlinear interactions between the waves drive energy to higher wavenumbers until they break, leading to enhanced turbulence far above the seafloor (Polzin et al., 1997; St. Laurent et al., 2001). This mechanism has been numerically simulated by Nikurashin and Legg (2011) and has been parameterized by Polzin (2009), based on the topography, the surface tide forcing, and the density stratification. Using these approaches, a modest fraction of the locally generated energy dissipates near small-amplitude but rough topography (about 30%; St. Laurent and Nash, 2003), and the rest is believed to radiate away as low modes. These approaches agree with available observational evidence, though more observations and numerical tests of the process at subcritical topography are warranted.

This paper reviews our efforts to understand the other extreme of supercritical topography, when the topography is relatively steep compared
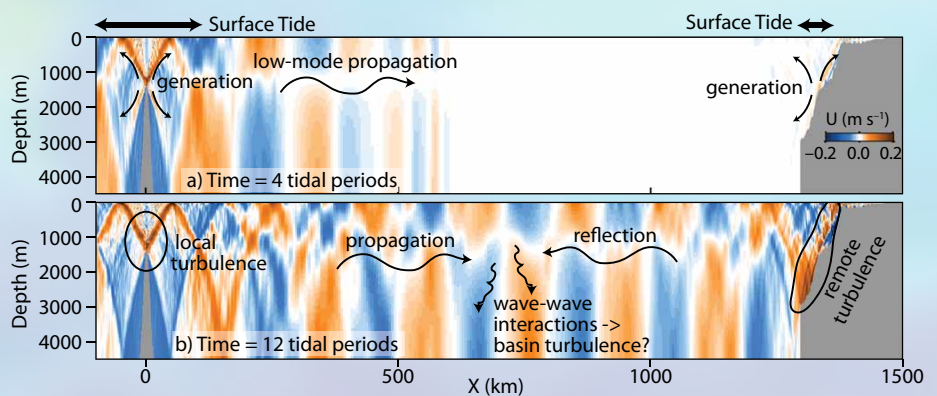

Figure 1. A numerical simulation of internal tide generation from a steep ridge (at x = 0 km) and a remote continental margin (at x = 1,300 km). Weaker generation from the continental slope reflects the weaker cross-slope tides there. Velocity is colored. The upper panel is early in the simulation to show the propagation of low-mode internal tides across the basin. The low modes travel faster than the high modes, which make up the "ray"-like character of the velocity closer to the ridge. Eventually, these rays would fill the whole basin if the resolution of the model permitted. The full solution shows the interaction of the propagating and reflected waves, and indicates the turbulence that would be observed at the remote continental slope.

to the internal tide rays. In this case, high-mode energy is believed to "break" directly near the topography due to the nonlinearity of the generation process itself. This breaking short circuits the energy cascade for the high-mode waves, and leads to spectacular localized turbulence. This paper reviews observations of these local breaking processes, and documents initial efforts to model and develop simple parameterizations of them. The observed processes are very nonlinear, and thus very sensitive to small changes in local forcing, so a large number of caveats come into play before we will fully understand turbulence at supercritical sites.

OBSERVATIONS

The breaking of internal waves at abrupt topography has now been observed at a number of locations, but the mechanism leading to this breaking has remained elusive. During the Hawaiian Ocean Mixing Experiment, at the Hawaiian Ridge, it was noted that there was strong turbulence near the seafloor and extending hundreds of meters into the water column (Figure 2; Aucan et al., 2006; Levine and Boyd, 2006; Klymak et al., 2008). These motions drove breaking internal waves that were up to 200 m tall, and mixing rates inferred from the size of the overturns were up to four orders of magnitude greater than open-ocean values at those depths.

Considering an event in detail (Figure 2), the turbulent overturns tend to be at the sharp leading face of rising density surfaces (isopycnals). This leading edge breaks, in this example, in two patches centered at 05:00 and 06:30. During the relaxation of the tide, there is a rebound at mid-depth (07:00) and sharp oscillations deeper (though these produce only modest turbulence). In all, the strong turbulence lasts over three hours; the remaining nine hours of the tidal cycle are relatively quiescent.

The main findings from the observations at Hawaii were:

1. Breaking waves were phase-locked to the surface tidal forcing.
2. Turbulence dissipation rates (a measure of the strength of the turbulence) scaled cubically with the spring-neap modulation of the surface-tide velocities.
3. The turbulence that had these characteristics was confined to within a few hundred meters of the seafloor; turbulence further aloft varied only weakly with the tidal forcing.

Similar observations have been made at the Oregon slope (Figure 3; Nash et al., 2007; Martini et al., 2011) and the South China Sea continental slope (Klymak et al., 2011). The turbulence at these locales was less than at Hawaii, but again depended on the tidal
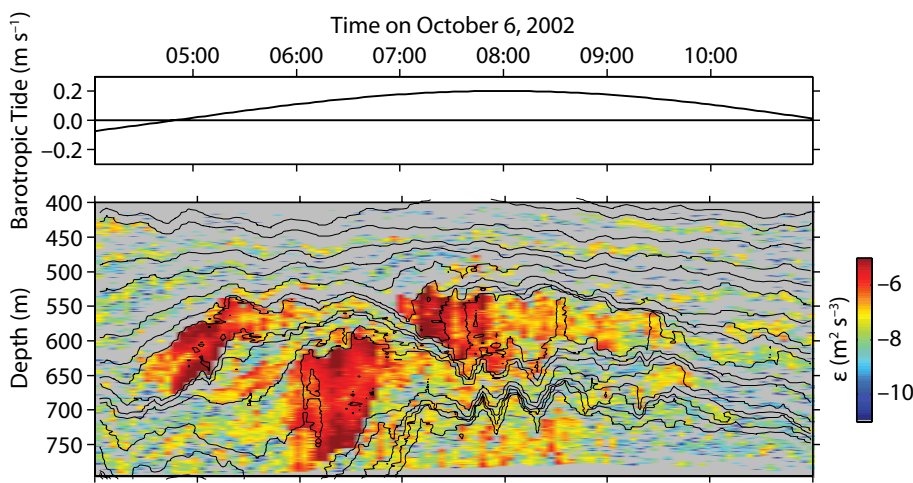

Figure 2. Observations of breaking waves made on the ridge crest between Oahu and Kauai, Hawaii (modified from Klymak et al., 2008), with the local surface tide plotted in the upper panel. The mooring was in 1,050 m of water; the bottom 250 m of the water column was not measured. Contours are density surfaces versus time during an onslope phase of the tide. Colors indicate turbulence dissipation rate, a measure of turbulent strength, inferred from the size of the breaking overturns in the waves, which reach almost 250 m tall near 06:00.

Jody M. Klymak (jklymak@uvic.ca) is Assistant Professor, School of Earth and Ocean Sciences, University of Victoria, Canada. **Sonya Legg** is Research Oceanographer, Atmospheric and Ocean Sciences Program, Princeton University, Princeton, NJ, USA. **Matthew H. Alford** is Principal Oceanographer, Applied Physics Laboratory, and Associate Professor, School of Oceanography, University of Washington, Seattle, WA, USA. **Maarten Buijsman** is Postdoctoral Research Scientist, Atmospheric and Ocean Sciences Program, Princeton University, Princeton, NJ, USA. **Robert Pinkel** is Professor and Associate Director, Marine Physics Laboratory, Scripps Institution of Oceanography, La Jolla, CA, USA. **Jonathan D. Nash** is Associate Professor, College of Earth, Ocean and Atmospheric Sciences, Oregon State University, Corvallis, OR, USA.

forcing. The phenomenology along these slopes is complicated by both rougher topography and the presence of shoaling internal tides that originated from elsewhere. At the Oregon slope, the strongest turbulence occurs during the transition from onslope to offslope flow, in contrast to the ridge crest at Hawaii, where the strongest turbulence occurs during the onslope flow. The difference in the timing of the turbulence likely depends on the local curvature of the topography and the mooring location relative to local generation sites, though a full explanation of the phenomenology of complex topography has not yet been accomplished. Perhaps the tallest breaking ocean waves yet observed occur in Luzon Strait, as depicted in Box 1; despite complicated bathymetry and tidal forcing, the end result is similar arrested lee wave behavior with greater than 500 m vertical scales.

TWO-DIMENSIONAL MODELING

Observations of turbulence near supercritical topography are quite difficult to link to the generation mechanism because it is difficult to sample the spatial scales fast enough to resolve the sharp tidal fronts that evolve. To help with interpretation, we have turned to numerical modeling at relatively high resolutions compared to most tidal models, but still coarse resolution compared to the turbulence (Legg and Klymak, 2008; Klymak and Legg, 2010). To date, we have simplified the problem by considering two-dimensional flows, but recent work is extending these efforts to three dimensions. By choosing appropriate tidal velocities and stratification to force over two-dimensional topography

(be it realistic or idealized), a picture emerges of the phenomenology of these breaking waves.

Phenomenology

Figure 4 is an example simulation that is meant to represent flow over the Hawaiian Ridge at Kauai Channel. It shows the lee waves that we believe are the primary turbulence-producing phenomena active at many supercritical topographies. During strong off-ridge flow (Figure 4b), a nonlinear lee wave is arrested at the sill, and it grows until it reaches a height exceeding 200 m and width spanning a few kilometers (Figure 4c). As the tide relaxes, the wave

is released and propagates on-ridge (Figure 4d). A similar structure forms on the other flank during the strong flow in the other direction. The shock-like character of this wave can be seen on the off-ridge edge, where the flow sharply rebounds analogously to the flow over an obstacle in a stream.

The simulation indicates why the site of observation can influence the phase of the tide when the turbulence occurs. If observations are made downslope of the topographic break (say, x = 3 km; Figure 5), then the turbulence will arrive with offslope flow. Conversely, if the observations are upslope (say, x = 1 km; Figure 5), then the turbulence
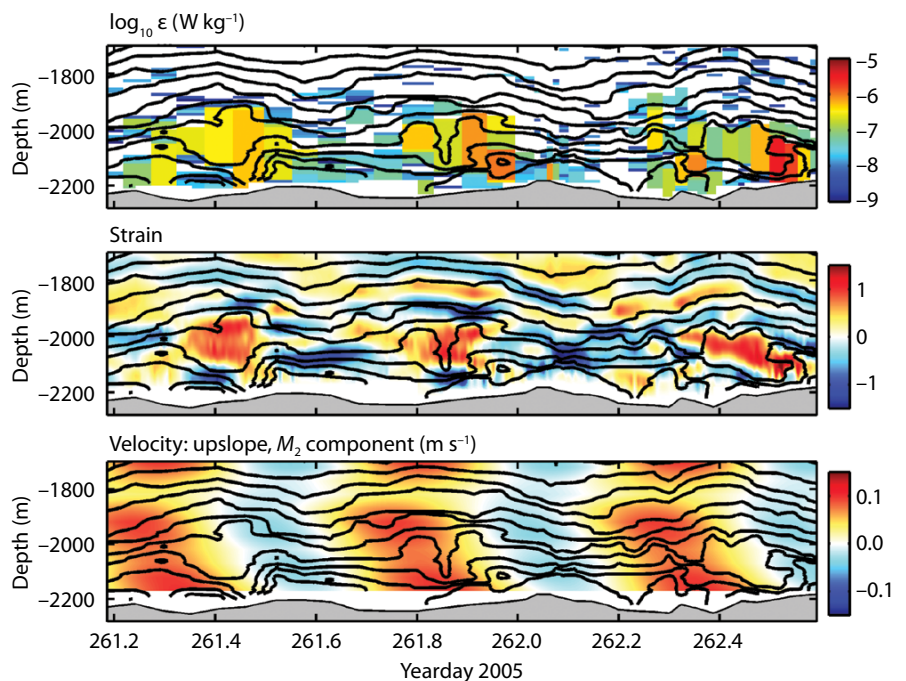
Figure 3. Breaking waves on the Oregon continental slope. Driven by a combination of barotropic and baroclinic tides that flow over small-scale bumps (of order 250–1,000 m horizontal scale) that overlie the otherwise steep continental slope, these waves occur on the leading edge of the downslope phase of the tide (modified from Nash et al. 2007). The upper panel is turbulence dissipation rate with isopycnals overlain; middle panel is isopycnal strain, measuring how stretched or compressed parts of the water column are by the internal tide; bottom panel is the upslope semidiurnal tidal velocities. The velocity shows downward phase propagation with time, indicating upwards propagation of energy from the seafloor. Local barotropic forcing is weak, and not well coupled to the local response.

BOX 1 | LUZON STRAIT

Situated between Taiwan and Luzon Island of the Philippines, Luzon Strait generates some of the largest-amplitude internal tides in the world (Alford et al., 2011). These internal tides result from the combination of strong barotropic tides (> 1 m s⁻¹) and ridge geometry that intersects the ocean's main thermocline at a depth where it most efficiently generates the energy-containing low modes. Luzon Strait is somewhat unique in that it consists of two ridges: a short one to the west, and a tall one to the east. In addition, the daily (diurnal) tide is stronger than the twice-a-day (semidiurnal) tide. While, in principle, a strong response at both diurnal and semidiurnal frequencies should ensue, the spacing of the two ridges promotes resonance of the semidiurnal internal tide between the ridges, and dissonance for the diurnal frequency (Jan et al., 2007; Echeverri et al., 2011; Buijsman et al., in press). As a result, the semidiurnal internal tide dominates the energetics between the ridges, producing waves that exceed 600 m in vertical displacement near steep topography.

Figure B1 shows the internal wave response during a 25-hour period in June 2011 (recent work of author Nash and colleagues). At this phase of the spring/neap cycle, the surface tide has strong diurnal inequality, with two westward velocity pulses every day, but just one to the east. The response of internal temperature surfaces reflects this imbalance. Although the wave (or low-frequency) nature of the flow is predominantly semidiurnal, turbulent overturning develops primarily after the strong diurnal velocity pulse to the east, producing 600 m tall waves and unstable overturns that exceed 500 m in height. In addition to these turbulent billows that pass our mooring as the barotropic flow reverses direction (e.g., 08:00–10:00 on June 16), also evident are short-period undulations higher in the water column that only occur once per day and are likely associated with instability of the strongest downslope flows between 04:00 and 08:00. This example highlights how semidiurnal and diurnal internal tides add together to produce a very strong wave and turbulent response that scales nonlinearly with the forcing.
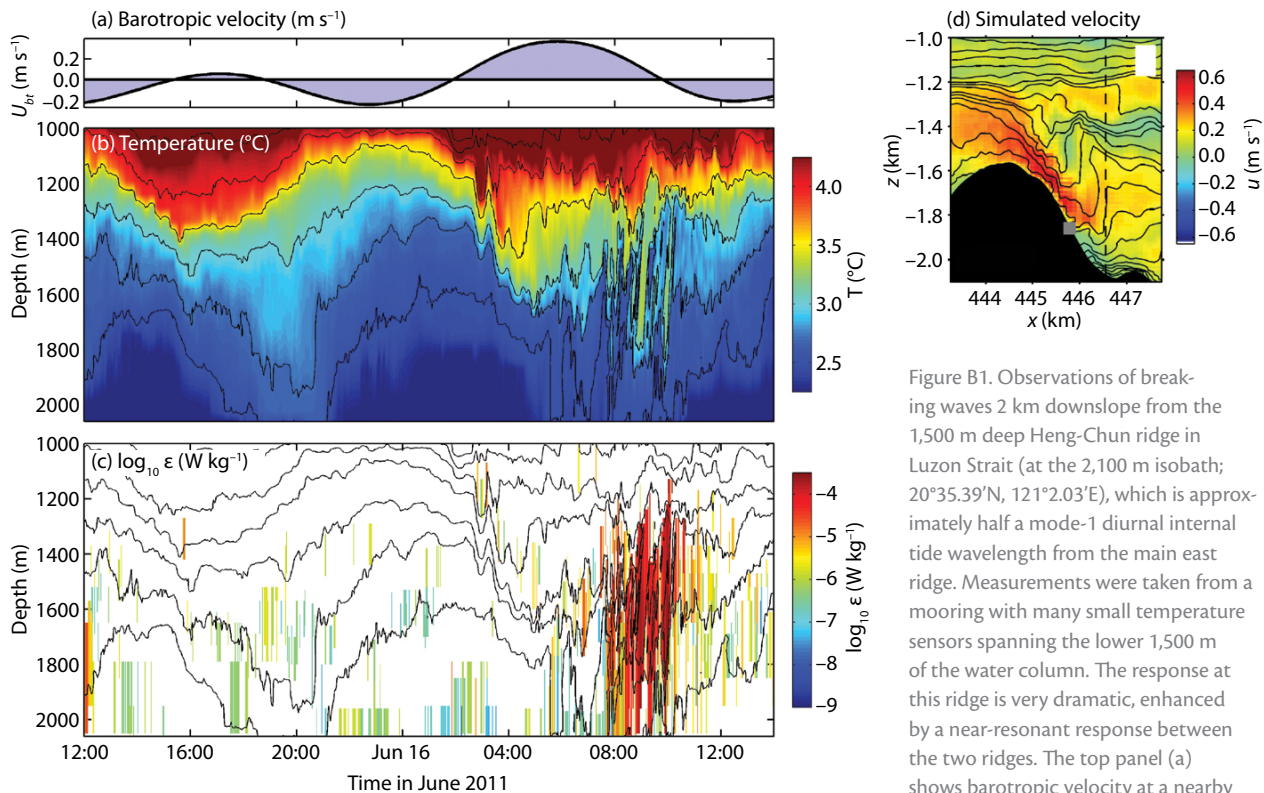

Figure B1. Observations of breaking waves 2 km downslope from the 1,500 m deep Heng-Chun ridge in Luzon Strait (at the 2,100 m isobath; 20°35.39'N, 121°2.03'E), which is approximately half a mode-1 diurnal internal tide wavelength from the main east ridge. Measurements were taken from a mooring with many small temperature sensors spanning the lower 1,500 m of the water column. The response at this ridge is very dramatic, enhanced by a near-resonant response between the two ridges. The top panel (a) shows barotropic velocity at a nearby ridge. Panel (b) shows a time series of temperature, from which the turbulence dissipation rate inferred from the size of breaking overturns in the flow (panel c); contours indicate constant temperature surfaces. Note the almost diagonal interleaving of warm and cold water starting at about 08:00. For context, panel (d) shows a two-dimensional numerical simulation by Buijsman et al. (in press), with colors and contours respectively representing velocity and temperature; the mooring location is in a region of intense wave breaking, as indicated by the dashed line. Note that the slope is extremely steep at this location, dropping approximately 300 m per kilometer!

will arrive during onslope flow as the trapped wave propagates on-ridge. At a simple topography like the Hawaiian Ridge, this process is quite clear. At more complex bathymetry like the Oregon slope (Figure 3), the phasing is probably dependent on the exact placement of the observations relative to smaller-scale changes in the bathymetry.

A fine-resolution simulation details what a typical lee wave looks like (Figure 5). A strong downslope flow accelerates with distance down the slope, but density layers peel off sequentially with depth, driving structures that look like breaking hydraulic jumps. The remainder of the jet separates partway down the slope, at the depth where it hits ambient water, and rebounds with strong vertical oscillations, again reminiscent of a hydraulic jump. The simulations are similar to observations in coastal fjords (Farmer and Armi, 1999; Klymak and Gregg, 2004) and to atmospheric simulations (Scinocca and Peltier, 1989), except that this motion only takes up 300 m of a 2,000 m deepwater column.

There is a comprehensive literature for nonlinear waves arrested at topography in situations where the flow has enough kinetic energy to lift water from most of the depth of the upstream basin over the obstacle. Such flows tend to make waves that are "low mode" or large compared to the water depth (Baines, 1995). For deep-ocean ridges, the flow is weak, and water is only withdrawn from near the obstacle crest. The vertical wavelength of the breaking waves is quite short compared to the water depth. It can be shown, however, that the physics is the same (Klymak et al., 2010a): if there is an off-ridge flow, the vertical mode with a horizontal phase speed close to that

of the flow speed at the ridge crest is arrested. This is the deep-ocean analog of a hydraulic jump in the lee of a rock in a river. The size of the wave can be

predicted from internal wave theory and compared to the size of waves generated in numerical simulations with very good agreement. The time it takes
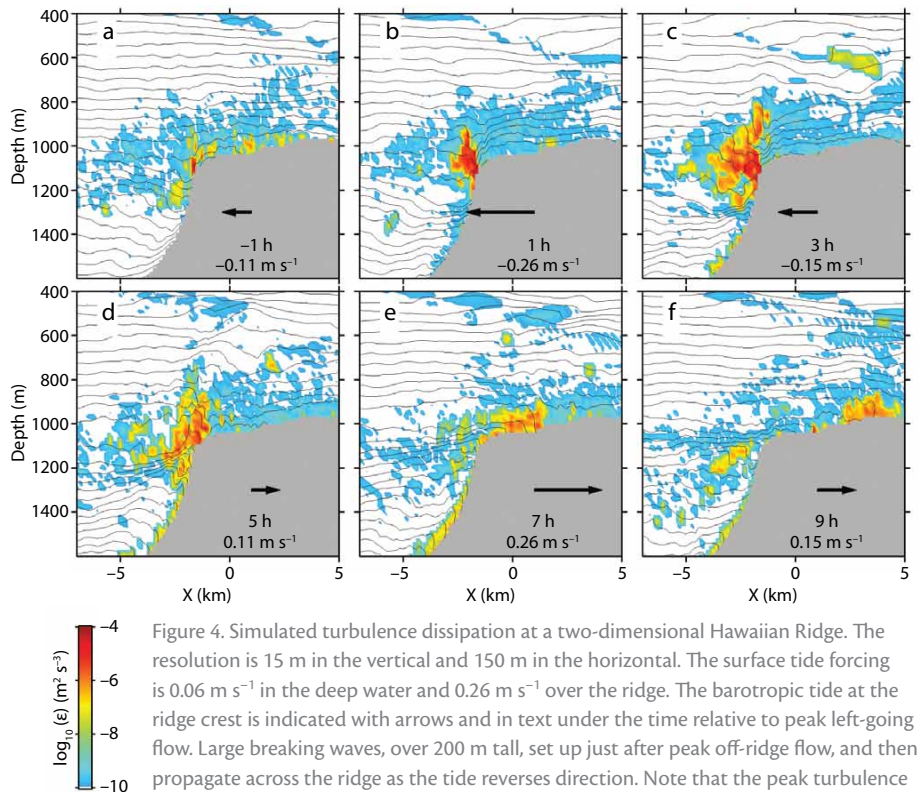

Figure 4. Simulated turbulence dissipation at a two-dimensional Hawaiian Ridge. The resolution is 15 m in the vertical and 150 m in the horizontal. The surface tide forcing is 0.06 m s⁻¹ in the deep water and 0.26 m s⁻¹ over the ridge. The barotropic tide at the ridge crest is indicated with arrows and in text under the time relative to peak left-going flow. Large breaking waves, over 200 m tall, set up just after peak off-ridge flow, and then propagate across the ridge as the tide reverses direction. Note that the peak turbulence is after peak flow, as it takes a finite amount of time for the lee wave to grow.
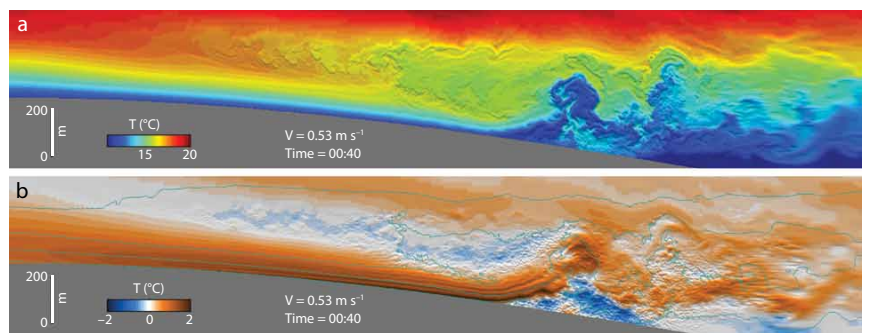

Figure 5. Detailed simulation of a breaking lee wave during peak off-ridge flow (this time to the right). Here, the vertical and horizontal resolution of the numerical model is 3 m, and the simulation is nonhydrostatic. Both panels have a one-to-one aspect ratio, and the crest of a smooth Gaussian topography is at 1,000 m depth in a 2,000 m deep water column. (a) Temperature (proxy for density), where large 200 m breaking waves can be seen both in the downslope flow zone, and where the strong off-ridge flow separates from the topography. Note that the color has been shaded by the vertical derivative of the temperature in order to accentuate the turbulent structure of the flow. (b) The cross-ridge velocity (red is off-ridge); the teal contours are temperature for comparison with (a). Again, the velocity has been shaded with the first difference in the vertical to accentuate turbulent structure.

for these waves to form depends on the topographic slope, with steeper slopes launching waves faster than gentler slopes. For an oscillating flow such as the tide, the finding is that the topography needs to be twice as steep as the internal wave slopes for oscillating lee waves to be effectively trapped and dissipative (Klymak et al., 2010b).

Recipe for Turbulence at Supercritical Topography

Here, we describe how the "arrested lee wave" concept allows for an analytical prediction of tidal turbulence and mixing near surpercritical topography based on the forcing, a simplified bathymetry, and the ocean's stratification. First, a linear theory can be used to predict the internal response of tidal flow over sharp topography (Llewellyn Smith and Young, 2003; St. Laurent et al., 2003). The predicted flow field has very sharp "beams" emanating from the ridge and

well-defined large-scale phase changes in the velocity on either side of these beams (Figure 6a). This theory predicts an internal wave energy flux away from the topography in each of the vertical modes (dashed line in Figure 6d).

Nonlinear numerical simulations of the same flow demonstrate similar features, particularly on the large scales (Figure 6b,c). However, the "beams" in the simulations are more diffuse, and some energy leaks out in higher-frequency (steeper) beams. As the forcing is increased (compare Figure 6c to b), the beams become even more diffuse. Diffuse beams indicate a loss of high-mode energy from the system, and this loss is quantified by noting that the energy flux at high modes does not agree with the linear theory (solid lines, Figure 6d and e). The stronger the forcing, the lower the mode where the disagreement starts, indicating a larger fraction of energy is dissipated.

To arrive at a dissipation rate, our recipe uses the observations above to determine the modes that break (Klymak et al., 2010b). The strongest flows at the top of the topography are compared to the phase speed of the modes. Fast modes are assumed to escape and form the radiated signal; slow modes are assumed to be trapped and form the dissipation. The stronger the forcing, the more modes are trapped (Klymak et al., 2010b). All the energy contained in the trapped modes is then assumed to transfer to turbulence locally. When compared to numerical simulations, this parameterization for the local turbulence dissipation rate is quite successful over a range of tidal forcing, bathymetry shape, stratifications, and latitudes (the Coriolis parameter strongly affects the energy put into the waves), so long as the topography is sufficiently supercritical (Figure 6f).

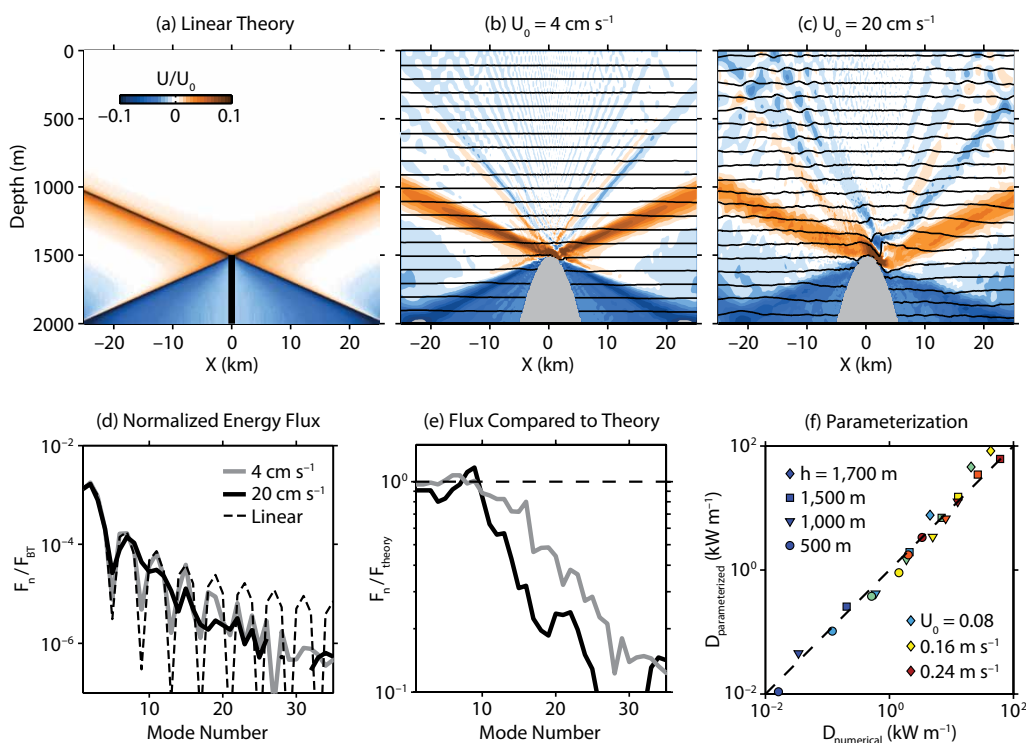An important finding of this analysis is that the local turbulence, while

Figure 6. (a) Snapshot of baroclinic (depth-mean removed) velocity from linear generation over a 500 m tall knife-edge ridge in 2,000 m of constant-stratification water, normalized by the barotropic forcing velocity. (b) Snapshot of the same configuration when the tidal forcing is 0.04 m s^{-1}, and (c) when it is 0.2 m s^{-1}. Note that the stronger forcing has less well-defined "beams" of energy radiating from the topography than the weaker, more linear forcing. (d) Comparison of the energy flux distributed by vertical mode number for (a)–(c) normalized by the energy flux of the barotropic wave. The 0.2 m s^{-1} case rolls off at lower mode numbers than 0.04 m s^{-1}, as also shown in (e). (f) The parameterization of Klymak et al. (2010b) predicts this fraction of energy as a function of forcing, topographic height, and stratification, usually within a factor of 1.5.

spectacular and locally important, is still a modest fraction of the energy removed from the surface tide. This can readily be discerned from Figure 1 or Figure 6, in which the full water-column motions that escape the ridges have significant energy. In fact, it requires very strong and nonlinear forcing for the local dissipation to even approach 10% of the internal tide energy budget at these sills. Thus, supercritical ridges are believed to be quite efficient radiators of energy, at least in the idealized forms considered so far in the modeling. A rough energy budget based on observations collected near Hawaii corroborates that idea (Klymak et al., 2006).

More Complicated Systems

Because supercritical topography seems to be efficient at generating internal tides without much local loss, the question stands as to the fate of that energy. Low modes will impact remote topography where they will scatter, reflect, or dissipate. If that topography is supercritical, such as at other underwater ridges or continental slopes, the same physics discussed above appears to apply: cross-topography flow generates turbulent lee waves that are phase-locked with the remote forcing, and a very similar parameterization is very effective at predicting the turbulence in these lee waves (recent work of author Klymak and colleagues). Predicting the turbulence at a remote ridge can become quite complicated if there is also local generation (Kelly and Nash, 2010). The phase between the local and remote forcing can change the turbulence predicted by an order of magnitude, and breaking lee waves are either suppressed or enhanced by the resonance.

Nowhere is this effect more clear than in a two-ridge system like Luzon Strait. In two-dimensions, a two-ridge version of the linear model can be constructed that shows strong interactions between the two ridges. The two ridges must be treated as a system, and the relative heights of the ridges and the distance between them greatly affect the response. The potential for resonance means that a larger fraction of the internal tide might go into local turbulence than might be the case for isolated ridges. Recent estimates of the local dissipation for Luzon Strait range from 20 to 40% of the energy lost from the surface tide (Alford et al., 2011; Buijsman et al., in press).

DISCUSSION

So far, we have seen that the internal tide at abrupt topography often breaks, short circuiting the process of cascading high-mode internal wave energy. This local breaking is vigorous, producing turbulent events that reach hundreds of meters tall, and orders of magnitude greater than open-ocean turbulence. The breaking is also phase-locked to the tide and strongly dependent on the strength of the forcing. Numerical modeling indicates that sources of this turbulence at many locations are lee waves arrested at the topographic breaks during off-ridge tidal flow, either driven by the local tide, or by remote tides. We have a parameterization for this process that works under a large range of forcing and topographies (i.e., Klymak et al., 2010b).

This progress in understanding the lee wave process does not preclude the importance of other processes that perhaps do not manifest themselves in idealized two-dimensional models. As indicated by MacKinnon and Winters

(2005) and Simmons (2008), there is potential for wave-wave interactions, particularly equatorward of the critical latitude where the Coriolis frequency is half the tidal frequency. It is also likely that there are wave-wave interactions local to the Hawaiian Ridge, as indicated in observations (Carter and Gregg, 2006) and as we have seen in our numerical models (Klymak et al., 2010b). However, it remains to be seen how important this energy pathway is near topography, and there are indications that it is modest in observations of the radiated tide (Alford et al., 2007).

There are a number of outstanding questions about the lee wave process and turbulence near supercritical topography. The first is, how good are estimates of the turbulent dissipation in these processes? There have been very few direct estimates of turbulence in these breaking waves; instead, the size of the wave is compared to the stratification it encompasses, and a dissipation rate inferred following Thorpe (1977). Detailed comparison between microconductivity and the size of the breaking waves at Hawaii had encouraging results (Klymak et al., 2008), as did comparisons between shear probes and breaking waves in Knight Inlet (Klymak and Gregg, 2004), but direct observations of turbulence dissipation at the microscale in these large mid-ocean lee waves are still needed. Similarly, questions arise as to the efficiency of the mixing in these breaking waves (i.e., what fraction of energy goes toward mixing density rather than turbulent friction processes?). Finally, the arguments in the papers summarized depend on numerical modeling that also assumes the turbulence is a function of the size of the breaking waves rather than more direct

estimates of dissipation, which require much more computing power. Some of these questions will be answered by forthcoming observations, particularly those planned in Luzon Strait. Others will require more detailed modeling, likely at the scale of large-eddy simulations, though these will be particularly challenging, given the broad scale of the internal tides (hundreds of kilometers) and the small eddy sizes (a few meters).

Much work to date, as described here, has been on two-dimensional idealizations of the flow. They are almost certainly over-simplifications, and three-dimensional models of these problems are being run (recent work of author Buijsman and colleagues). Funneling of flow by constrictions can greatly enhance the lee waves, so deciding on appropriate forcing and topography when applying the simple parameterizations discussed above is not trivial. Similarly, we have considered flow over topography that is largely supercritical with respect to the tide, except at the ridge crest. However, a lot of topography is more complicated than this, with significant roughness that can interact with the tides, or substantial near-critical regions that also convert tidal energy efficiently into turbulence (Eriksen, 1982; McPhee and Kunze, 2002).

Despite these substantial caveats, we are attempting to create a global map of dissipation due to local forcing at supercritical topography. There are estimates of tidal currents, stratification, and topography, so this problem should be tractable. To make progress, a number of challenging assumptions need to be made when applying the parameterization suggested here globally. What scale should the topography be smoothed over to decide on its height? What tidal velocity should be used? How to account for the funneling of flows through constrictions? How to account for narrow topography that may not result in substantial generation (Johnston and Merrifield, 2003)? Finally, if incoming internal tides from afar are important for local turbulence, either enhancing or suppressing it, then accurate maps of global internal tidal energy, perhaps at low modes, will be needed before a global estimate can be made (Kelly and Nash, 2010). This task will prove challenging as tides are advected by large-scale currents and changes in stratification (Rainville and Pinkel, 2006), making their predictability questionable (Nash et al., 2012, in this issue), so it is possible that global coarse internal tide models will need to be used to quantify this remote forcing (Simmons et al., 2004, and Arbic et al., 2012, in this issue).

REFERENCES

Alford, M.H. 2003. Redistribution of energy available for ocean mixing by long-range propagation of internal waves. *Nature* 423:159–162, http://dx.doi.org/10.1038/nature01628.

Alford, M.H., J.A. MacKinnon, Z. Zhao, R. Pinkel, J. Klymak, and T. Peacock. 2007. Internal waves across the Pacific. *Geophysical Research Letters* 34, L24601, http://dx.doi.org/10.1029/2007GL031566.

Alford, M.H., J.A. MacKinnon, J.D. Nash, H. Simmons, A. Pickering, J.M. Klymak, R. Pinkel, O. Sun, L. Rainville, R. Musgrave, and others. 2011. Energy flux and dissipation in Luzon Strait: Two tales of two ridges. *Journal of Physical Oceanography* 41:2,211–2,222, http://dx.doi.org/10.1175/JPO-D-11-073.1.

Arbic, B.K., J.G. Richman, J.F. Shriver, P.G. Timko, E.J. Metzger, and A.J. Wallcraft. 2012. Global modeling of internal tides within an eddying ocean general circulation model. *Oceanography* 25(2):20–29, http://dx.doi.org/10.5670/oceanog.2012.38.

Aucan, J., M.A. Merrifield, D.S. Luther, and P. Flament. 2006. Tidal mixing events on the deep flanks of Kaena Ridge, Hawaii. *Journal of Physical Oceanography* 36:1,202–1,219, http://dx.doi.org/10.1175/JPO2888.1.

Baines, P.G. 1995. *Topographic Effects in Stratified Flows*. Cambridge University Press, 500 pp.

Balmforth, N., G. Ierley, and W. Young. 2002. Tidal conversion by subcritical topography. *Journal of Physical Oceanography* 32:2,900–2,914, http://dx.doi.org/10.1175/1520-0485(2002)032<2900:TCBST>2.0.CO;2.

Bell, T.H. 1975. Lee waves in stratified flows with simple harmonic time dependence. *Journal of Fluid Mechanics* 67:705–722, http://dx.doi.org/10.1017/S0022112075000560.

Buijsman, M., S. Legg, and J.M. Klymak. In press. Double ridge internal tide interference and its effect on dissipation in Luzon Strait. *Journal of Physical Oceanography*.

Carter, G.S., and M.C. Gregg. 2006. Persistent near-diurnal internal waves observed above a site of M2 barotropic-to-baroclinic conversion. *Journal of Physical Oceanography* 36:1,136–1,147, http://dx.doi.org/10.1175/JPO2884.1.

D'Asaro, E.A. 1995. Upper-ocean inertial currents forced by a strong storm. Part II: Modeling. *Journal of Physical Oceanography* 25:2,937–2,952, http://dx.doi.org/10.1175/1520-0485(1995)025<2937:UOICFB>2.0.CO;2.

Echeverri, P., T. Yokossi, N. Balmforth, and T. Peacock. 2011. Tidally generated internal-wave attractors between double ridges. *Journal of Fluid Mechanics* 669:354–374, http://dx.doi.org/10.1017/S0022112010005069.

Eriksen, C.C. 1982. Observations of internal wave reflection off sloping bottoms. *Journal of Geophysical Research* 87(C1):525–538, http://dx.doi.org/10.1029/JC087iC01p00525.

Farmer, D.M., and L. Armi. 1999. Stratified flow over topography: The role of small-scale entrainment and mixing in flow establishment. *Proceedings of the Royal Society of London A* 455:3,221–3,258, http://dx.doi.org/10.1098/rspa.1999.0448.

Garrett, C., and E. Kunze. 2007. Internal tide generation in the deep ocean. *Annual Review of Fluid Mechanics* 39:57–87, http://dx.doi.org/10.1146/annurev.fluid.39.050905.110227.

Henyey, F.S., J. Wright, and S.M. Flatté. 1986. Energy and action flow through the internal wave field. *Journal of Geophysical Research* 91:8,487–8,495, http://dx.doi.org/10.1029/JC091iC07p08487.

Jan, S., C. Chern, J. Wang, and S. Chao. 2007. Generation of diurnal K_1 internal tide in the Luzon Strait and its influence on surface tide in the South China Sea. *Journal of Geophysical Research* 112, C06019, http://dx.doi.org/10.1029/2006JC004003.

Johnston, T.M.S., and M.A. Merrifield. 2003. Internal tide scattering at seamounts, ridges, and islands. *Journal of Geophysical Research* 108, 3180, http://dx.doi.org/10.1029/2002JC001528.

Kelly, S., and J. Nash. 2010. Internal-tide generation and destruction by shoaling internal tides. *Geophysical Research Letters* 37, L23611, http://dx.doi.org/10.1029/2010GL045598.

Klymak, J.M., M.H. Alford, R. Pinkel, R.C. Lien, Y.J. Yang, and T.Y. Tang. 2011. The breaking and scattering of the internal tide on a continental slope. *Journal of Physical Oceanography* 41:926–945, http://dx.doi.org/10.1175/2010JPO4500.1.

Klymak, J.M., and M.C. Gregg. 2004. Tidally generated turbulence over the Knight Inlet sill. *Journal of Physical Oceanography* 34:1,135–1,151, http://dx.doi.org/10.1175/1520-0485(2004)034<1135:TGTOTK>2.0.CO;2.

Klymak, J.M., and S.M. Legg. 2010. A simple mixing scheme for models that resolve breaking internal waves. *Ocean Modelling* 33:224–234, http://dx.doi.org/10.1016/j.ocemod.2010.02.005.

Klymak, J.M., S. Legg, and R. Pinkel. 2010a. High-mode stationary waves in stratified flow over large obstacles. *Journal of Fluid Mechanics* 644:312–336, http://dx.doi.org/10.1017/S0022112009992503.

Klymak, J.M., S. Legg, and R. Pinkel. 2010b. A simple parameterization of turbulent tidal mixing near supercritical topography. *Journal of Physical Oceanography* 40:2,059–2,074, http://dx.doi.org/10.1175/2010JPO4396.1.

Klymak, J.M., J.N. Moum, J.D. Nash, E. Kunze, J.B. Girton, G.S. Carter, C.M. Lee, T.B. Sanford, and M.C. Gregg. 2006. An estimate of tidal energy lost to turbulence at the Hawaiian Ridge. *Journal of Physical Oceanography* 36:1,148–1,164, http://dx.doi.org/10.1175/JPO2885.1.

Klymak, J.M., R. Pinkel, and L. Rainville. 2008. Direct breaking of the internal tide near topography: Kaena Ridge, Hawaii. *Journal of Physical Oceanography* 38:380–399, http://dx.doi.org/10.1175/2007JPO3728.1.

Legg, S., and J.M. Klymak. 2008. Internal hydraulic jumps and overturning generated by tidal flow over a tall steep ridge. *Journal of Physical Oceanography* 38:1,949–1,964, http://dx.doi.org/10.1175/2008JPO3777.1.

Levine, M.D., and T.J. Boyd. 2006. Tidally-forced internal waves and overturns observed on a slope: Results from the HOME survey component. *Journal of Physical Oceanography* 36:1,184–1,201, http://dx.doi.org/10.1175/JPO2887.1.

Llewellyn Smith, S.G., and W.R. Young. 2003. Tidal conversion at a very steep ridge. *Journal of Fluid Mechanics* 495:175–191, http://dx.doi.org/10.1017/S0022112003006098.

MacKinnon, J.A., and K.B. Winters. 2005. Subtropical catastrophe: Significant loss of low-mode tidal energy at 28.9°N. *Geophysical Research Letters* 32, 15605, http://dx.doi.org/10.1029/2005GL023376.

Martini, K.I., M.H. Alford, E. Kunze, S.M. Kelly, and J.D. Nash. 2011. Observations of internal tides on the Oregon continental slope. *Journal of Physical Oceanography* 41:1,772–1,794, http://dx.doi.org/10.1175/2011JPO4581.1.

McPhee, E.E., and E. Kunze. 2002. Boundary layer intrusions from a sloping bottom: A mechanism for generating intermediate nepheloid layers. *Journal of Geophysical Research* 107, 3050, http://dx.doi.org/10.1029/2001JC000801.

Munk, W., and C. Wunsch. 1998. Abyssal recipes II: Energetics of tidal and wind mixing. *Deep Sea Research Part I* 45:1,977–2,010, http://dx.doi.org/10.1016/S0967-0637(98)00070-3.

Nash, J.D., M.H. Alford, E. Kunze, K. Martini, and S. Kelley. 2007. Hotspots of deep ocean mixing on the Oregon continental slope. *Geophysical Research Letters* 34, L01605, http://dx.doi.org/10.1029/2006GL028170.

Nash, J.D., E. Kunze, J.M. Toole, and R.W. Schmitt. 2004. Internal tide reflection and turbulent mixing on the continental slope. *Journal of Physical Oceanography* 34(5):1,117–1,134, http://dx.doi.org/10.1175/1520-0485(2004)034<1117:ITRATM>2.0.CO;2.

Nash, J.D., E.L. Shroyer, S.M. Kelly, M.E. Inall, T.F. Duda, M.D. Levine, N.L. Jones, and R.C. Musgrave. 2012. Are any coastal internal tides predictable? *Oceanography* 25(2):80–95, http://dx.doi.org/10.5670/oceanog.2012.44.

Nikurashin, M., and S. Legg. 2011. A mechanism for local dissipation of internal tides generated at rough topography. *Journal of Physical Oceanography* 41:378–395, http://dx.doi.org/10.1175/2010JPO4522.1.

Polzin, K.L. 2009. An abyssal recipe. *Ocean Modelling* 30(4):298–309, http://dx.doi.org/10.1016/j.ocemod.2009.07.006.

Polzin, K.L., J.M. Toole, J.R. Ledwell, and R.W. Schmitt. 1997. Spatial variability of turbulent mixing in the abyssal ocean. *Science* 276:93–96, http://dx.doi.org/10.1126/science.276.5309.93.

Rainville, L., and R. Pinkel. 2006. Baroclinic energy flux at the Hawaiian Ridge: Observations from the R/P *FLIP*. *Journal of Physical Oceanography* 36:1,104–1,122, http://dx.doi.org/10.1175/JPO2882.1.

Scinocca, J.F., and W.R. Peltier. 1989. Pulsating downslope windstorms. *Journal of the Atmospheric Sciences* 46:2,885–2,914, http://dx.doi.org/10.1175/1520-0469(1989)046<2885:PDW>2.0.CO;2.

Simmons, H.L. 2008. Spectral modification and geographic redistribution of the semi-diurnal internal tide. *Ocean Modelling* 21:126–138, http://dx.doi.org/10.1016/j.ocemod.2008.01.002.

Simmons, H.L., R.W. Hallberg, and B.K. Arbic. 2004. Internal wave generation in a global baroclinic tide model. *Deep Sea Research Part II* 51:3,069–3,101, http://dx.doi.org/10.1016/j.dsr2.2004.09.015.

St. Laurent, L.C., H.L. Simmons, and S.R. Jayne. 2002. Estimating tidally driven mixing in the deep ocean. *Geophysical Research Letters* 29(23), 2106, http://dx.doi.org/10.1029/2002GL015633.

St. Laurent, L.C., J.M. Toole, and R.W. Schmitt. 2001. Buoyancy forcing by turbulence above rough topography in the abyssal Brazil Basin. *Journal of Physical Oceanography* 31:3,476–3,495, http://dx.doi.org/10.1175/1520-0485(2001)031<3476:BFBTAR>2.0.CO;2.

St. Laurent, L.C., and J.D. Nash. 2004. An examination of the radiative and dissipative properties of deep ocean internal tides. *Deep Sea Research Part II* 51:3,029–3,042, http://dx.doi.org/10.1016/j.dsr2.2004.09.008.

St. Laurent, L.C., S. Stringer, C. Garrett, and D. Perrault-Joncas. 2003. The generation of internal tides at abrupt topography. *Deep Sea Research Part I* 50:987–1,003, http://dx.doi.org/10.1016/S0967-0637(03)00096-7.

Thorpe, S.A. 1977. Turbulence and mixing in a Scottish loch. *Philosophical Transactions of the Royal Society of London A* 286:125–181, http://dx.doi.org/10.1098/rsta.1977.0112.